Journal of Engineering Research and Applied Science
Available at www.journaleras.com
Volume 11 (2), December 2022, pp 2156-2170
ISSN 2147-3471 © 2022

Evaluation of Gümüştuğ Antimonite (Torul, Gümüşhane/Türkiye) Mineralization with Soil Geochemistry and Multivariate Geostatistical Studies

Alaaddin Vural[1*], Bilal Cicek[2]

[1,*] Gümüşhane University, Faculty of Engineering and Natural Science, Department of Geology, Gümüşhane, Türkiye
[2] Gümüşhane University, Graduate Education Institute,Gümüşhane, Türkiye

Accepted 15 November 2022

Abstract

This study aims to investigate the evaluation of Gümüştuğ antimonite (Torul, Gümüşhane/Türkiye) mineralization with soil geochemistry and multivariate geostatistical studies, and to shed light on the understanding of the embedded ore geometry. In this context, 56 soil samples were taken from the field with a square method and analyzed for Sb, Au, Ag and related trace elements. The statistical properties of the obtained element concentrations are determined by descriptive statistical parameters and multivaria geoistatic methods. By calculating the threshold values of the elements and factors, element distribution maps in the ore zone were created both on the elementary basis and on a factoral basis. As a result of the study, a positive correlation was found between As and Sb, Au, between Au and Bi, between Zn and As, Cd, Sb, and between Cu and Zn, Ag, Co, Mn, As, Au, Bi elements. According to the factor analysis, it was understood that the As, Au and Sb elements were included in the same factor and therefore behave under the control of the same physicochemical conditions, and that the factor that controls the behavior of these three elements was originally the same and was associated with hydrotermal alteration processes. When the distribution map of the Factor 3, which defines As, Au and Sb for the study area, was found to be concentrated in the north and west/southwest segment of the fields and the work to be carried out in these areas for Sb and Au ores in these areas, it was concluded that the realization in the regions will give satisfactory results in the context of the mine search.

Keywords: Gümüştuğ Antimonite, Soil Geochemistry, Multivariate Geostatistic, Torul (Gümüşhane), Türkiye

1. Introduction

The study area is in and around Gümüştuğ (Torul-Gümüşhane/Türkiye) within the southern part of the Eastern Pontide Orogenic Belt (Figure 1). Anatolia is a geography where many mining activities have been carried out since ancient times [1,2], and Gümüşhane is an important mining region that was named Argyropolis in the past due to the mineral deposits it hosts [3]. Today, it is one of the most important cities that contribute to Türkiye's economy with mining. It is thought that there are many mineral deposits still waiting to be discovered in the region. For this reason, many mineral exploration studies have been carried out in the region [4–6]. Mineral exploration activities are a very difficult process and soil geochemistry studies have an important place in these processes [7–12]. A short-term mining activity was carried out in the Gümüştuğ site in the past, but the site was abandoned because the size of the mineralization and its reserve were not considered satisfactory. Considering the intense hydrothermal alteration patterns and mineralizations in and around the site, Gümüştuğ antimonite mineralization has the potential to be a mineral deposit. Soil geochemistry study was carried out in the site, considering that the geometry of a possible buried mineralization in the field can be revealed by using the surface data, especially with the soil geochemistry study. For this purpose, field work was carried out in the site, soil samples were taken to cover the area where mineralization also developed and analyzes of trace elements associated with antimonit were carried out. From these data, distribution maps of the elements were plotted with the help of different statistical methods and suitable drilling locations were suggested for the site.

* Corresponding author:
ORCID: https://orcid.org/0000-0002-0446-828X
Email: alaaddinvural@hotmail.com

2. Material and Method

2.1. Geology of the Eastern Black Sea Region and Study Area

The region, in which the study area is located, is within the Eastern Black Sea Tectonic Union (EBSTU) (Pontid Tectonic Unions) of the Black Sea Tectonic Union (BTU) [13]. Since the Late Cretaceous rocks in the EBTU show variations in the northern and southern parts, the EBTU is divided into southern and northern regions [14]. [15] and [16] divided the Eastern Black Sea magmatic arc into three subclasses from north to south, namely the northern zone, the southern zone and the axial zone, according to different magmatism, tectonism and sedimentological periods.

The basement rocks of the EBSTU are composed of Early Carboniferous metamorphic rocks [17] and Late to Early Carboniferous plutonic rocks [18–26]. These basement rocks are uncomformably overlain by Early and Middle Jurassic volcano-sedimentary rocks [27,28] and crosscutting plutonic rocks of Mid to Late Jurassic [29,30]. Late Jurassic to Early Cretaceous period is characterized with extensive carbonate deposits corresponding to the stability period from a magmatic and tectonic perspective [31]. Late Cretaceous units consist of plutonic, volcanic and sedimentary rocks [32–39]. Cenozoic units consist of volcanic, plutonic and sedimentary units [40,41,50–55,42–49]. The youngest units in the region are travertine, terraces, and alluviums.

The study area is in the South Zone close to the North-South Zone transition of the EBTU (Figure 1). In the region, units of different ages and different lithologies crop out from the Paleozoic to the end of the Tertiary [56–58]. The oldest units in the study area are Permo-Carboniferous plutonic rocks (Artabel Granitoid) [20,59,60]. These rocks are overlain by Early-Middle Jurassic volcano-sedimentary rocks (Zimonköy Formation) with erosional unconformity [56,61]. The Late Jurassic-Early Cretaceous Berdiga Formation conformably overlies these units. The Berdiga Formation is overlain by Late Cretaceous Kermutdere Formation. This formation starts with sandy limestones at the base, continues with burgundy limestones and ends with volcano-sedimentary series. The unit is also cut by Late Cretaceous andesite and basalt [35,57,62]. Eocene Alibaba Formation unconformably overlies Kermutdere Formation and consists of andesite, basalt and pyroclastics of them and intercalated sediments. All these units were cut by the Lutetian (44±0.2 Ma) Avliyana Granitoid [51,57,63] (Figure 1). The youngest units of the study area are Quaternary alluvium, talus and travertine [64,65].

2.2. Mineralization and Alteration

Antimonite mineralization has developed in a structurally controlled hydrothermal vein type, 1.5-2 km SW of Gümüştuğ (Avliyana) village, in the country rock that makes tectonic contact with the Avliyana Granitoid and in the fractures and cracks of the granitic rock. With the effect of Gümüştuğ Granitoid in the field, hydrothermal alteration has developed in the country rocks where the intrusives are in contact. Although there are many alteration areas developed in the immediate vicinity of the antimonite mineralization, it was observed that the antimonite mineralization developed within a narrow area. The mineralization has developed in a tectonic line trending N60-85W and inclined to 70-75 E within the alteration zone and in secondary fractures and cracks connected to this line [57,58,66]. The mineralization zone is a forested area and there is moderate soil development on the mineralization, and good soil development in some parts.

2.3. Fieldwork, collection of samples, preparation for analysis and analysis

Recognition of the units outcropping in the region, contact relations with other rocks, structural conditions and stratigraphic features were determined by field studies. In order to determine the distribution of antimonite mineralization on the surface and to determine the characteristics of other antimonite-related elements in the site and their relations with each other, the study area was divided into grids on the topograpic map, and 56 samples were collected by going to the points allocated to grids at intervals of 100 meters by GPS (Figure 1). Soil samples taken were left to dry for about 2 weeks in a room temperature environment without moisture to remove their natural moisture. Then, by keeping them in an oven at 60°C for 8 hours, their natural moisture was completely removed. Soil samples were crushed and sieved through 100 mesh sieves, approximately 30 g of powder samples were obtained, bagged, and sent to the ACME laboratory (Canada) and analyzed. The remaining samples were used for Loss on Ignition (LOI) and pH measurements at Gümüşhane University, Geological Engineering Geochemistry Laboratory. Details of LOI and pH measurements are given in Vural ve Çiçek [67]. Major and trace element analyzes of soil samples were performed with Inductively Coupled Plasma Atomic Emission Spectrometer, and rare earth element (REE) analyzes were performed with Inductively Coupled Plasma Mass Spectrometer (ICP-MS). ACME Laboratory

standards (STD DS11 and STD OREAS 262 standards) were used in the analysis of the elements. The results of the analyzes were checked with routine accuracy testing procedures. 0.25 g of powder samples were taken and dissolved in four different acids (hydrochloric acid, sulfuric acid, hydrogen peroxide, nitric acid) and analyzed for Mo, Cu, Pb, Zn, Ag, Ni, Co, Mn, Fe, As, Au, Sr, Cd, Sb, Bi, V, La, Cr, Ba, Sc and Hg. Au, Ag and Hg element concentrations were calculated as µg/kg, Mn, Fe elements as % (percent) and other elements as mg/kg.

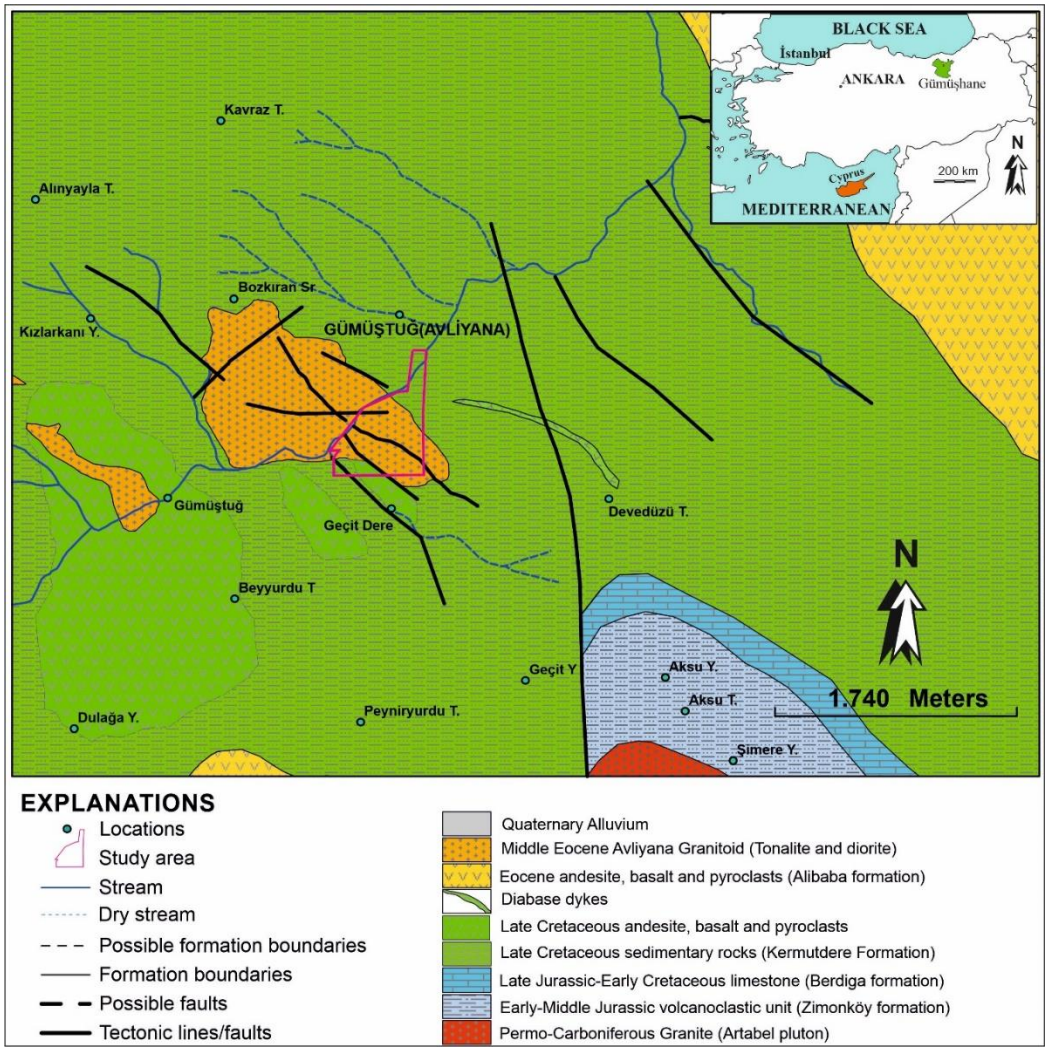

Figure 1. Study site location and geology map (after [56] and [57])

2.4. Data Analytics

Analysis results were statistically evaluated with IBM SPSS Statistics 22 and Microsoft Excel package programs, and ArcGIS v.10.5 program was used in spatial statistics studies. In this context, descriptive statistics (mean, median, maximum, minimum etc., distribution characteristics (normality tests), relations with each other (correlation, factor analysis), spatial distribution (inverse distance weighting, variogram) of the data were investigated.

2.4.1. Descriptive Statistics

Within the scope of descriptive statistical studies, parameters such as minimum, maximum, arithmetic, and geometric mean, median, and their standard deviation of element concentrations in the soil were calculated. These parameters were also used in the threshold value calculations for the elements.

2.4.2. Correlation

Correlation coefficients were calculated to determine the direction, degree and importance of the relationship between elements. The correlation coefficient is denoted by "r" and the r value takes values between -1 and +1. If the r value takes values close to -1, it is determined that there is a negative relationship between the variables, and a positive relationship is determined if it takes values close to

+1. If the r value is close to zero, it is concluded that there is no relationship between the two variables. The most widely used correlation analyzes are Pearson and Spearman correlation analyzes. Pearson correlation analysis is used if the variables are obtained with a proportional or interval scale and conform to the normal distribution, and if the variables are obtained with a proportional or interval scale but do not comply with the normal distribution, Spearman correlation analysis is used.

2.4.3. Determination of Data Distribution Character

It is generally tried to determine whether the data show a normal distribution or not, by means of central tendency parameters, histogram, box diagrams, parametric and non-parametric test methods. In this study, the mentioned evaluations were made, and Kolmogrow-Smirnov and Shapiro-Wilk tests were also applied to the data. Normality Tests help us to check whether the data we have fits the normal distribution. All these parameters and the data were evaluated separately, and the distribution character of the data was decided according to most of the parameter results.

2.4.4 Factor Analysis

Factor analysis aims to obtain a small number of identifiable significant variables from many variables that measure the same construct. In geochemistry, it enables many data to be reduced and the data to be easily evaluated by grouping (assigning to a factor) many elements that exhibit similar behavior and/or those that are similarly affected by similar conditions. Before the factor analysis is performed, the suitability of the data for factor analysis is tested. Two methods are commonly used to evaluate the suitability of factor analysis of data. These are the Bartlett test and the Kaiser-Meyer-Olkin (KMO) sample adequacy measurement. KMO's test must be greater than 0.5 for factor analysis to be appropriate. If the P value < 0.05 for Bartlett's test, the data set is suitable for factor analysis. The most common factor analysis method is principal component analysis (PCA). Deciding on the number of factors that best describes the fundamental relationship between variables is subjective. This requires balancing between two conflicting needs. There is a need to find a simple solution with the fewest possible factors and as much variance annotation as possible with the original data set. Once the number of factors has been determined, the resulting factors should be interpreted. To aid this process, the factors are "rotated". This does not change the underlying solution, but rather simply presents the pattern of charges. After this stage, the factors obtained are named and interpreted.

2.4.5. Threshold Calculation

The threshold value is the value calculated according to the values in the data set and accepted as the anomaly initial limit of the data set. In this study, the threshold value was calculated using the arithmetic mean±2 standard deviation (M±2SD), geometric mean±2 standard deviation (GeO±2SD), median±2 median absolute deviation (M±MAD) methods and concentration-number method, and the obtained threshold values were compared.

2.4.5.1. Mean ± 2 SD

The mean±2 standard deviation is widely used in calculating the threshold value for normal and/or near-normally distributed data. The mean and standard deviation are calculated as follows, respectively.

$$\mu = \frac{1}{N}\sum_{i=1}^{N} x_i. \quad (1)$$

$$\sigma = \sqrt{\frac{1}{N}\sum_{i=1}^{N}(x_i - \mu)^2}. \quad (2)$$

where, μ is the arithmetic mean of the population, σ is the standard deviation, N is the number of populations, and xi represents each data in the population. For the sample population, $\bar{x}$ is used for meaning and s' for standard deviation, respectively.

2.4.5.2. Geometric Mean ±2 SD

It is more appropriate to use geometric mean instead of arithmetic mean for data that do not show normal distribution. It is obtained by taking the nth order root of the product of n elements in a data set, as follow:

$$\mu_g = \sqrt[n]{x_1 \times x_2 \times \ldots \times x_n} \quad (3)$$

where, μ_g geometric mean, x1, x2, x3,…xn, denotes the data. Since it is difficult to calculate the geometric mean with this formula, it is more useful to take the exponential mean of the logarithms of the data. It is generally useful for simple data and negative data is not used. The geometric standard deviation, on the other hand, is the exponent of the square root of the mean of the square of the difference of the data from the geometric mean, and in its simplest form, it is calculated as follows:

$$\sigma_g = exp\sqrt{\frac{\sum_{i=1}^{n}(ln\frac{x_i}{\mu_g})^2}{n}} \quad (4)$$

where σ_g corresponds to the geometric standard deviation.

2.4.5.3. Median ±2 Median Absolute Deviation (M±2MAD)

One of the problems encountered for geochemical data is the difficulty of achieving ideal distributions, despite the application of many methods for transforming non-normally distributed data into normal distribution. In such cases, one of the methods used in the calculation of the threshold (T), especially in order to reduce the effect of extreme values, is to calculate the median absolute deviation (MMS) and add 2MAD to the median value of data set (M±2MAD).

2.4.5.4. Concentration-Number (C-N) Method

The Concentration-Number Fractal Method (C-N) was proposed by [68] and developed by [69]. The calculation method is given below:

$$N(\geq \rho) = F\rho^{-\beta} \quad (5)$$

where -β is the Benchmark exponent for the fractal size of the concentration distribution. ρ represents the element concentrations and N represents the number of samples belonging to a concentration value greater than or equal to ρ. In addition, the log-log plot of N(≥ρ)-ρ shows different curved line segments showing the "-β" value in ratios representing different concentration ranges. The advantage of the C-N method is the use of raw data. Therefore, it provides fast and effective interpretation.

2.5. Spatial Geostatistical Methods

Valuation methods of mineral deposits can be considered in two parts: Geostatistical methods and Areal geometric methods. In geometric methods, values such as grade, distance, and thickness can take place randomly among the variables and it is accepted that there is no relationship between them. Triangle, polygon, section, and section block method are among the geometric methods. In geostatistical methods, correlation is sought between samples depending on the distance. Generally, the measured values of points that are closer to each other in terms of distance are also close to each other [70]. With this method, which is based on the logic of regional variables, data belonging to unsampled points are obtained with calculations called estimation by using the values of the points sampled in a region. The spatial geostatistical methods are briefly mentioned below.

2.5.1. Variyogram

A variogram is a relationship function that depends on distance and direction. It is used to analyze the structural characteristic of spatial data and to define the degree of spatial correlation. Values of regional variables are determined only at the sampled points of the relevant region. The unsampled points are determined by the estimation method.

2.5.2. Variogram Function

The Variogram Function is calculated as the variance of the difference between the values of the random variable as follows:

$$2\gamma(h) = \text{var}\,[Z(x) - Z\,x+h)] \quad (6)$$

where, 2γ(h): variyogram fonksiyonu; Z(x): The value of the random variable at point x; Z(x+h): The value of the random variable at a distance h from the point x.

The variogram gives information about regional variables. The isotropy, homogeneity, regularity, and impact distance of the regional variables examined in a mineralization can be determined by the variogram function. For example, calculations can be made in 4 cardinal directions on two-dimensional data, such as N-S (0°), NW-SE (45°), E-W (90°) and NE-SW (135°). If the variogram does not change according to the directions, the regional variable is said to be isotropic. The regularity and continuity of regional variables depend on the general behavior of the variogram. The main features of the function of the variogram are as follows:

In cases where the distance is zero (h=0), the variogram is also equal to zero γ(0) = 0.

Since the variogram function is the variance of the difference between two random variables, it cannot be a negative value γ(h) ≥ 0. If the expression is calculated negative, it means that the selected variogram function is not suitable. The variogram function is symmetrical γ(h) ≥ γ(-h).

2.5.3. Modeling of Data and Validity of Models

The variogram is calculated for the unit distance called lag and its multiples. If the samples have a random distribution, the mean distance between samples is taken as the lag distance. The mean distance value is calculated by taking the square root of the total area with the selected samples divided by the number of samples. The tolerance to be used for the lag distance is taken to be at most half of the lag distance. In the study, the anisotropy of the region was examined by drawing variogram graphs on the vertical axis. The variograms were calculated at 45° intervals to determine the anisotropy of the anomalies in the area. ArcGIS v.10.5 software was used for modeling the data. There are different methods for determining concentration distributions

in the field. The most common ones are Kriging and inverse distance weighting (IDW). In this study, the inverse distance weighting method was preferred. The IDW Method is the most well-known for deterministic models other than probability cases in the plotting of distribution maps of elements. The IDW interpolation model is the oldest spatial prediction method. This method is the easiest deterministic interpolation method compared to other methods. There are multiple decision-making methods involved in realizing model parameters. It provides the advantage of quick and easy information about interpolated surfaces [8]. It is preferred because of its easy and fast use. Although there are several IDW methods, the most well-known is "Shaperd's Method". The “p- prime” value (power function) is included in the calculation of the IDW method. In IDW, as the exponent increases, there is less and less effect on distant points. While the IDW gives good results when frequent and equally weighted sampling points are concerned, the results obtained are not always accurate when it comes to complex relationships with the environment under study. Considering the frequent and equal/close to equal sampling points in the study area, the p-power value was taken as 2. Element distribution maps were created using the Inverse Distance Weighting Method with the ArcGIS v.10.5 package program.

3. Results

3.1. Geochemical and Geostatistical Studies

56 soil samples taken from the mineralization area were analyzed for certain trace elements (Mo, Cu, Pb, Zn, Ag, Co, Mn, As, Au, Cd, Sb, Bi, Hg) and descriptive statistics of soil samples (minimum, maximum, median, etc.) are given in Table 1.

Table 1. Descriptive Statistics of the soil samples

	N	Min.	Max.	Mean	Std. Dev.	Varians	Skewness	Kurtosis
Mo	56.00	0.45	2.34	1.05	0.47	0.22	0.87	0.01
Cu	56.00	31.34	190.68	81.01	43.13	1860.59	1.01	-0.12
Pb	56.00	9.38	42.41	25.46	8.56	73.22	0.23	-0.80
Zn	56.00	45.60	111.60	75.93	13.20	174.17	0.12	0.04
Ag	56.00	26.00	254.00	107.84	55.82	3115.70	0.49	-0.63
Ni	56.00	13.90	107.80	45.86	25.75	663.18	0.80	-0.23
Co	56.00	14.90	55.10	28.18	11.57	133.82	0.74	-0.80
Mn	56.00	0.05	0.13	0.08	0.02	0.00	0.38	-0.22
Fe	56.00	3.70	5.78	4.57	0.49	0.24	0.17	-0.58
As	56.00	3.70	20.50	10.98	4.14	17.16	0.57	0.05
Au	56.00	0.90	8.50	3.74	1.92	3.69	0.44	-0.83
Sr	56.00	34.80	75.50	49.54	9.70	94.12	0.91	0.47
Cd	56.00	0.06	0.34	0.18	0.06	0.00	0.19	-0.27
Sb	56.00	0.40	41.02	4.41	6.67	44.54	3.57	16.18
Bi	56.00	0.27	10.47	2.09	2.22	4.92	1.93	3.60
V	56.00	83.00	140.00	105.07	9.90	98.10	1.12	2.74
La	56.00	10.40	24.60	13.95	3.16	9.97	1.89	3.38
Cr	56.00	19.20	123.10	54.48	24.43	596.90	0.78	0.43
Ba	56.00	72.10	591.60	152.14	87.08	7583.54	3.65	14.90
Sc	56.00	5.60	16.40	9.30	1.96	3.84	1.05	2.61
Hg	56.00	8.00	87.00	24.89	10.97	120.32	3.30	18.19

3.2. Distribution character of data

The distribution characteristics of the data were determined by using box diagram, histogram graphs, Q-Q diagrams, skewness, and kurtosis parameters as well as normality test. The Normality Test was evaluated by considering the Kolmogorov-Smirnov method since the number of samples was more than 30 (grey area). Elements with a significance coefficient of 5% and above are considered to have a normal distribution (light gray-bold point; Pb, Zn, Ag, Mn, Fe, Cd) (Table 2).

Q-Q, % diagrams, box and histogram graphs were created for the elements. With the graphs and diagrams obtained, it was examined in which interval the elements showed intense distribution, their normal distribution states, and their skewness. With all these data, the distribution character of each element was determined by considering the degree of skewness and kurtosis. Considering these data; it was

concluded that while Pb, Zn, Mn, Fe, Cd, Bi, V and Sc elements showed normal distribution, Mo, Cu, Ag, Ni, Co, As, Au, Sr, La, Cr, Ba and Hg elements show non-normal distribution (for detailed evaluation, see [71].

Table 2. Kolmogorov-Smirnov and Shapiro-Wilk Normality Tests

	Kolmogorov-Smirnov[a]			Shapiro-Wilk		
	Statistics	N	Sig.	Statistics	N	Sig.
Mo	0.168	56	0.000	0.899	56	0.000
Cu	0.223	56	0.000	0.859	56	0.000
Pb	0.087	56	**0,200***	0.970	56	0.182
Zn	0.053	56	**0,200***	0.994	56	0.995
Ag	0.094	56	**0,200***	0.949	56	0.020
Ni	0.174	56	0.000	0.910	56	0.000
Co	0.185	56	0.000	0.873	56	0.000
Mn	0.100	56	**0,200***	0.975	56	0.289
Fe	0.080	56	**0,200***	0.980	56	0.459
As	0.159	56	0.001	0.938	56	0.006
Au	0.132	56	0.016	0.947	56	0.015
Sr	0.146	56	0.005	0.929	56	0.003
Cd	0.102	56	**0,200***	0.978	56	0.387
Sb	0.336	56	0.000	0.554	56	0.000
Bi	0.313	56	0.000	0.728	56	0.000
V	0.106	56	**0.184**	0.930	56	0.003
La	0.196	56	0.000	0.787	56	0.000
Cr	0.139	56	0.009	0.926	56	0.002
Ba	0.317	56	0.000	0.561	56	0.000
Sc	0.109	56	0.095	0.940	56	0.008
Hg	0.178	56	0.000	0.734	56	0.000

3.3. Correlation Analysis

Pearson and Spearman correlation coefficients were calculated to determine the relationships of the elements with each other (Table 3). However, Spearman correlation coefficients were considered as most of the data did not show normal distribution. According to Spearman correlation coefficients, a positive correlation was observed between Mo and Cu, Co, Mn elements, and a negative correlation was observed between Mo and Sb. There was a positive correlation between Cu and Zn, Ag, Co, Mn, As, Au and Bi. A positive correlation was observed between Zn and As, Cd and Sb. A positive correlation was seen between Co and Mn and between Mn and Bi. There was a positive correlation between As and Au and Sb, and a positive correlation between Au and Bi.

Table 3. Pearson and Spearman Correlation coefficients (Pearson green, Spearman pink)

	Mo	Cu	Pb	Zn	Ag	Co	Mn	As	Au	Cd	Sb	Bi
Mo	**1**	**0.47****	0.24	-0.23	0.25	**0.62****	**0.49****	-0.17	-0.01	0.03	**-0.72****	0.37**
Cu	**0.61****	**1**	**0.48****	0.18	**0.67****	**0.84****	**0.61****	**0.46****	**0.59****	0.36**	-0.21	**0.83****
Pb	0.32*	**0.64****	**1**	**0.59****	**0.70****	**0.46****	0.33*	0.41**	0.22	**0.84****	0.03	**0.55****
Zn	-0.16	0.27*	0.60**	**1**	0.42**	0.14	0.18	**0.55****	0.29*	**0.63****	**0.57****	0.09
Ag	0.42**	**0.71****	**0.71****	0.37**	**1**	**0.49****	0.34**	**0.58****	**0.61****	**0.51****	0.15	**0.66****
Co	**0.58****	**0.93****	**0.57****	0.20	**0.62****	**1**	**0.79****	0.20	0.37**	0.34*	-0.37**	**0.71****
Mn	0.35**	**0.64****	0.32*	0.26	0.39**	**0.72****	**1**	0.24	0.34**	0.30*	-0.31*	**0.55****
As	-0.21	0.27*	0.34*	0.59**	0.37**	0.14	0.20	**1**	**0.69****	0.35**	**0.55****	0.38**
Au	0.02	**0.46****	0.20	0.31*	**0.54****	0.40**	0.34*	**0.65****	**1**	0.04	0.28*	**0.58****
Cd	0.080	**0.48****	**0.85****	**0.66****	**0.48****	0.42**	0.29*	0.31*	0.01	**1**	0.12	0.39**
Sb	-0.43**	-0.24	-0.12	0.20	0.06	-0.36**	-0.31*	**0.55****	0.42**	-0.13	**1**	-0.24
Bi	**0.63****	**0.75****	**0.56****	0.03	**0.78****	**0.67****	**0.48****	0.10	0.35**	0.33*	-0.22	**1**

**. 0.01 significant coefficient; *. 0.05 significant coefficient

3.4. Threshold Calculation

The threshold values (ED) of the elements in the study area were calculated using the mean, geometric mean, median and concentration-number (C-N) methods. While the threshold value calculated with the arithmetic mean can be used for normally distributed data, it is stated by many researchers that the threshold values obtained by geometric mean and median+2 median absolute deviation methods, in which the effect of extreme values are minimized, are more accurate for data that do not show normal distribution [11]. The C-N method, in which raw data can be used directly, is also one of the preferred and recommended methods for calculating equal values [72]. It is known that especially in cases where several geochemical processes develop together, the basic values of the elements and the threshold values are exposed to a lot of influence, the threshold values determined by fractal methods (e.g. C-N) are known to work in areas with low anomaly contrasts and in situations where low threshold values are in question [68]. Threshold values calculated for the study area are given in Table 4.

Table 4. Threshold values calculated for the field

Element	Mean	M+2SD	Geometric Mean	GeO+2SD	Median	M+2MAD	C-N
Mo	1.05	1.28	0.95	2.85	0.95	1.82	2.24
Cu	81.01	77.16	71.46	77.15	60.60	153.46	77.24
Pb	25.46	23.20	23.98	24.10	25.31	39.27	38.18
Zn	75.90	76.42	74.78	70.22	76.40	96.87	88.64
Ag	108.0	105.15	92.97	90.85	98.50	200.69	164.44
Co	28.20	25,22	26.07	20.14	23.70	47.91	36.23
Mn	0.083	1598.28	0.08	1617.24	0.08	1637.03	1564.88
As	11.0	12.16	10.19	12.22	20.20	17.19	16.16
Au	3.70	4.18	3.23	3.02	3.45	7.01	6.18
Sr	49.50	54.24	48.67	45.15	46.35	64.61	55.15
Cd	0.18	0.22	0.17	0.16	0.18	0.28	0.33
Sb	4.41	4.88	2.42	2.04	1.85	12.57	10.80
Bi	2.09	2.96	1.36	1.18	1.17	5.44	3.74
Sc	9.30	8.72	9.11	8.72	9.10	12.18	10.18
Hg	25.0	22.40	23.18	25,62	24.50	38.33	24.26

Tablo 5. KMO and Bartlett's Test

Kaiser-Meyer-Olkin Measure of Sampling Adequacy.		0.769
Bartlett's Test of Sphericity	Approx. Chi-Square	598.522
	df	66
	Sig.	0.000

3.5. Factor Analysis

Differentiation is observed in the behavior of the elements according to the physicochemical conditions. This differentiation depends on the factors affecting the physicochemical conditions. Factor analysis is one of the most effective methods used to determine the elements that show association according to factors in geochemical studies. Factor analysis is commonly used in cases where too many parameters are examined together in the data set and/or to detect path finder elements that are effective in the exploration for elements found in low concentrations in nature, such as gold. In the study, factor analysis was performed to determine the relations of the elements with each other, and to determine the path finder elements for gold and to plot the distribution map. Principal component analysis, which is the most common, was preferred in the study. The suitability of the data for factor analysis was evaluated with the KMO and Bartlett's test. The KMO test result was 0.769 and the Barlett's test sig. value was found to be less than 0.05, and data set factor analysis was performed (Table 5). As a result of factor analysis, three factors with eigenvalue greater than 1 were determined (Table 6). To minimize the relations of the factors with each other, the factors were rotated perpendicular to each other with the Varimax method (Table 7). The cumulative variance value of the three factors was determined as 79.55% (F1: 37.613+F2: 22.194+F3: 19.746), (Table 7). Elements falling within the same factor are shown in bold in Table 7 and circled in

Figure 2. Summary statistics of As, Au and Sb elements falling into Factor-3 are given in Table 8.

Table 6. Total Variance Explained

Component	Initial Eigenvalues			Extraction Sums of Squared Loadings			Rotation Sums of Squared Loadings		
	Total	% of Variance	Cumulative %	Total	% of Variance	Cumulative %	Total	% of Variance	Cumulative %
1	5.44	45.324	45.324	5.44	45.324	45.324	4.51	37.613	37.613
2	2.58	21.499	66.824	2.58	21.499	66.824	2.66	22.194	59.806
3	1.53	12.729	79.553	1.53	12.729	79.553	2.37	19.746	79.553
4	.898	7.480	87.033						
5	.378	3.149	90.182						
6	.304	2.535	92.717						
7	.277	2.312	95.029						
8	.240	1.999	97.028						
9	.124	1.031	98.059						
10	.109	.909	98.968						
11	.085	.705	99.674						
12	.039	.326	100.000						
Extraction Method: Principal Component Analysis.									

Table 7. Rotated Component Matrix

	Components		
	1	2	3
Mo	**0.768**	-0.107	-0.326
Cu	**0.896**	0.289	0.102
Pb	0.479	**0.806**	0.024
Zn	-0.004	**0.824**	0.363
Ag	**0.714**	0.367	0.325
Co	**0.892**	0.233	-0.011
Mn	**0.681**	0.168	0.053
As	0.070	0.383	**0.816**
Au	0.436	-0.034	**0.830**
Cd	0.232	**0.928**	-0.071
Sb	-0.352	-0.037	**0.807**
Bi	**0.866**	0.112	0.029

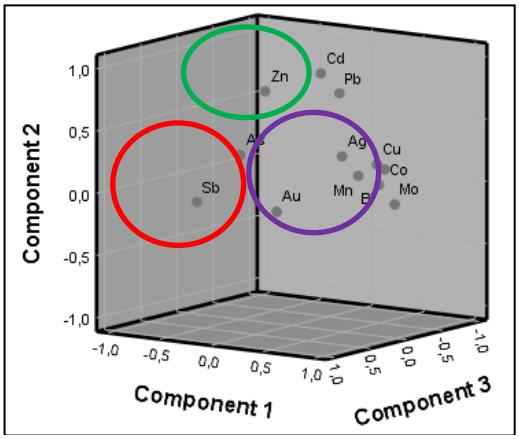

Figure 2. Display of components in three dimensions

Table 8. Factor 3 (As, Au and Sb) descriptive statistics

Statistics	As (ppm)	Au (ppb)	Sb (ppm)	F3
Median	3.739	10.984	4.406	6.376
Variance	17.159	3.691	44.540	21.8
Maxsimum	20.50	8.50	41.02	23.34
Minimum	3.70	0.90	0.40	1.67
Standart Deviation	4.142	1.921	6.674	4.24
Median absolute deviation	17.190	7.006	12.573	12.25

For the distribution map to be created, the factor value of each sampling point was calculated with the following formulation:

Factor 1=0.768*Mo+0.896*Cu+0.714*Ag+0.892*Co+0.681*Mn+0.866*Bi

Faktör 2=0.8206*Pb+0.824*Zn+0.928*Cd

Faktör 3=0.816*As+0.830*Au+0.807*Sb

3.6. Element Distribution Maps

In the plottign of element distribution maps, IDW interpolation method, which is the most applied among deterministic models, was used (for Kriging method, see [71]) (Figures 3 and 4). In the distribution maps made for Mo and Cu elements, it was observed that Mo element was concentrated in the Southwest and Southeast parts of the study area, and Cu element was concentrated in the East and West parts of the area. In the distribution maps of Pb and Zn elements, it is seen that the Pb element is concentrated in the northern and southern parts of the study area. It has been observed that Zn element is concentrated in the North-Northeast and Southwest parts of the field (Figure 3). In the distribution map of Ag, it is seen that it is concentrated in the East of the study area and in the western parts close to the center, and it is locally concentrated in the northern part of the area. As to Co, it has been observed that Co is concentrated in the East and Southwest parts of the study area (Figure 3). According to the element distribution maps, although Mn is common throughout the study area, it is seen that the distribution decreases in the North-Southeast and central parts of the area. As is concentrated from the center of the field to the North. Au is generally concentrated in the North-Northeast parts of the study area. Cd is concentrated at the northeastern and southwestern ends of the field. In the distribution maps, the Sb element is generally concentrated in the midwest and northern parts of the study area, while the Bi element is concentrated in the central east and west of the area. The Hg element is concentrated in the Northwest and Southeast parts of the study area, while the Fe element is concentrated in the East and West of the study area.

When the distribution maps prepared for the factors obtained as a result of factor analysis are examined, it is seen that Factor 1 presents an intense distribution in the central and SW sections of the study area. In the Factor 2 distribution map, the density is evident in the north and center of the study area. In the factor 3 distribution map, on the other hand, concentration is seen in the central part of the study area and in the west of the central part, and very little in the NW part (Figure 4).

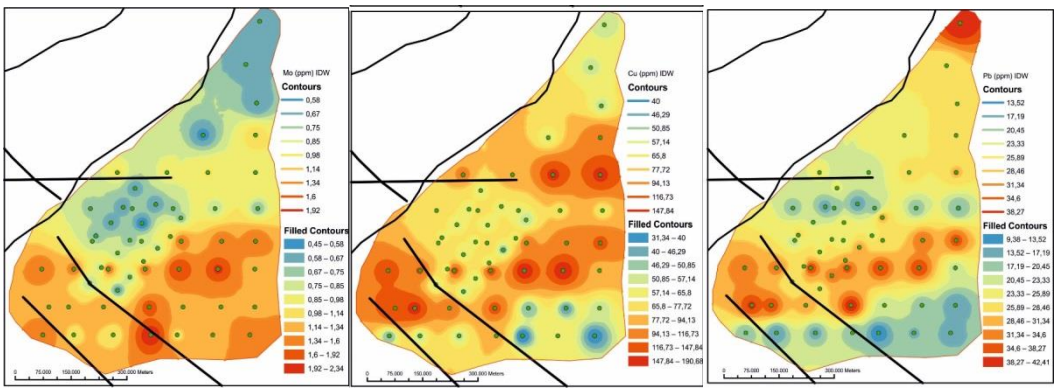

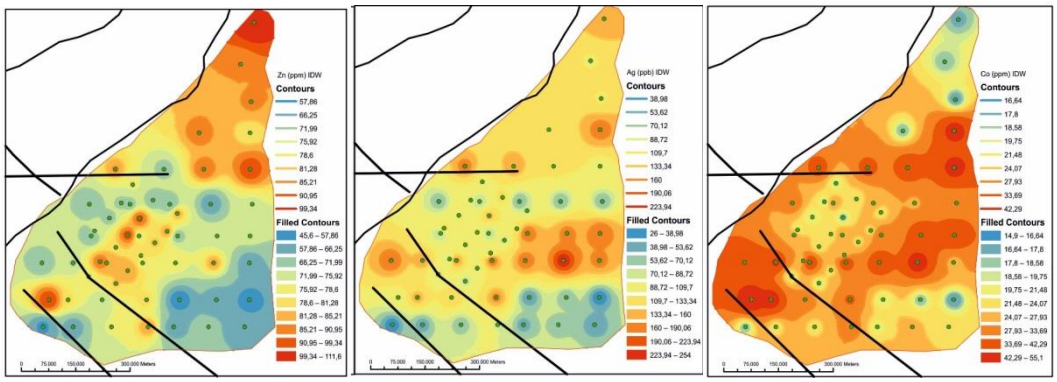

Figure 3. Distribution maps of Mo, Cu, Pb, Zn, Ag, Co, Mn, As, Au, Cd, Sb and Bi elements

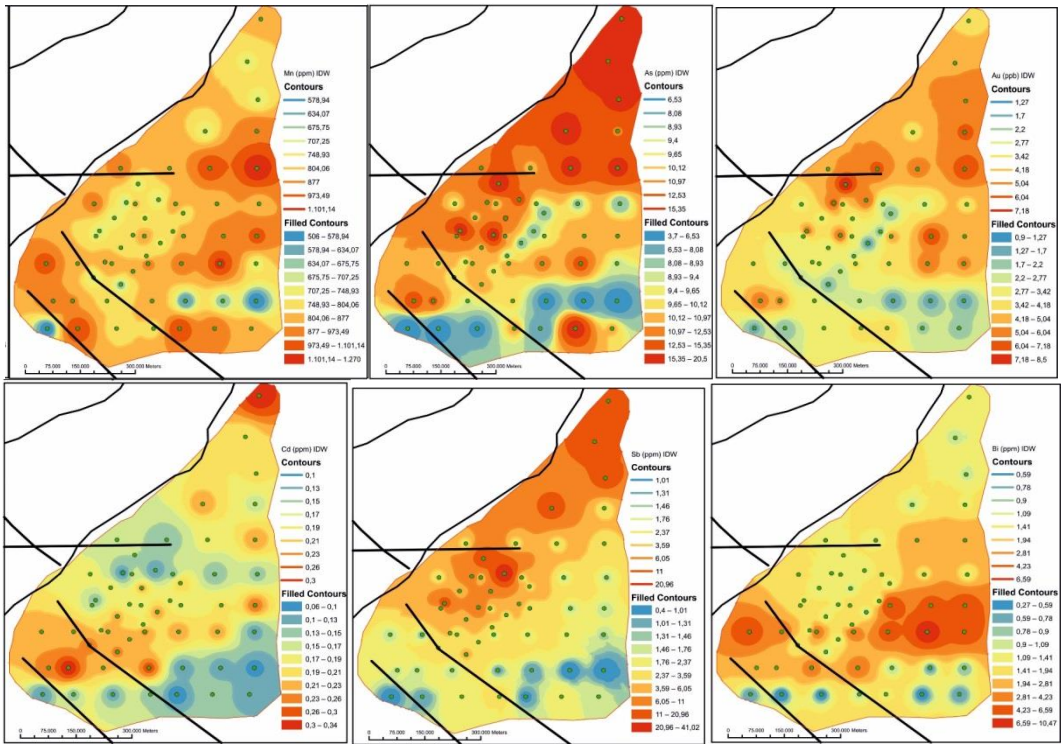

Figure 3. (continue)

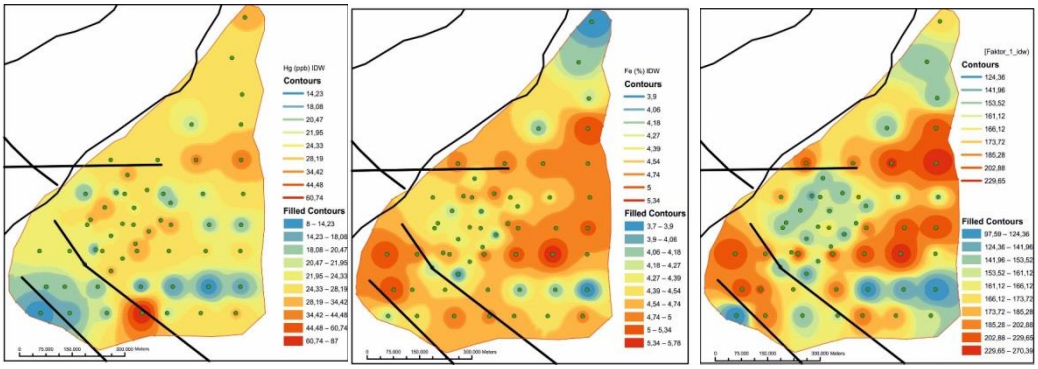

Figure 4. Distribution maps of Hg, Fe, Factor 1, Factor 2, and Factor 3

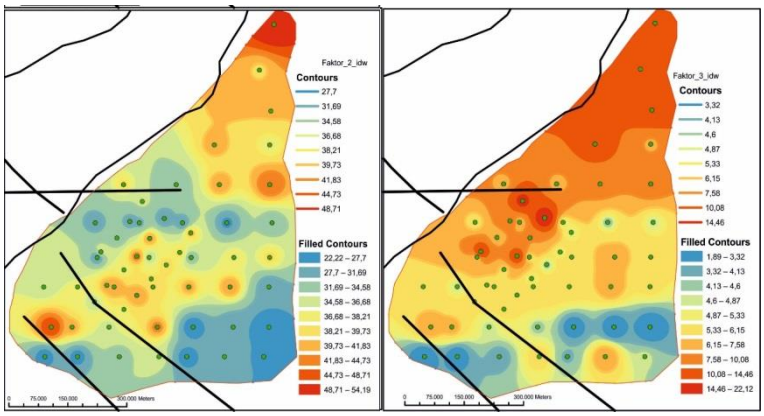

Figure 4. (Continue)

4. Conclusion and Recommendations

With this study, it is aimed to determine the two-dimensional distribution-orientation of the Gümüştuğ (Torul, Gümüşhane/Türkiye) antimonite mineralization with soil geochemistry studies and to contribute to future studies. As a result of soil geochemistry and geochemical studies, it has been determined that there is a positive, but not very strong, relationship between Sb and Ag and Au, and that Ag and Au concentrations are slightly higher than Clark values in the area where Sb is concentrated. Considering the soil geochemistry findings, it was observed that Mo, Cu, Ag, Co, Mn and Bi elements in Factor 1 were concentrated in the east and west of the study area. It is seen that Pb, Zn and Cd elements in factor 2 are concentrated in the north and southwest regions of the study area. In the Factor 3 distribution map, which includes As, Au and Sb elements, concentration is seen in the north and west/southwest parts of the field. It is thought that it will be beneficial to carry out the detailed exploration studies to be planned in the field and the drilling studies to be carried out according to the soil geochemistry data. So, it is expected that the studies to be carried out will yield satisfactory results.

Acknowledgements

This study was supported by Gümüşhane University Scientific Research Projects Coordinatorship (Project No: 19.F5114.01.02). The authors thank the relevant editor and anonymous referees for their contributions.

References

[1] Vural A, Kaya S, Başaran N, Songören OT. Anadolu Madenciliğinde İlk Adımlar. Ankara, Türkiye: Maden Tetkik ve Arama Genel Müdürlüğü, MTA Kültür Serisi-3; 2009.

[2] Kaya S, Başaran N, Songören T, Vural A, Kayadibi Ö. Evaluations Related To Mining Archeology (Geo-Archeology) in Amasya City. 7th International Symposium on Eastern Mediterranean Geology. 2010.

[3] Vural A, Erşen F. Eski Gümüşhane (Argyropolis) Manganez Yataklarının Jeolojik Ve Jeokimyasal Özellikleri. 66. Türkiye Jeoloji Kurultayı. Ankara, Türkiye: 2013:162–163.

[4] Özdoğan K. Karadağ (Torul-Gümüşhane) ve Yakın Çevresinin Jeolojisi-Mineralojisi-Petrografisi ve Maden Zuhurlarının Jenetik İncelenmesi. Selçuk Üniversitesi, Fen Bilimleri Enstitüsü, Doktora Tezi, Konya: 1992.

[5] Lermi A. Midi (Karamustafa/Gümüşhane, KD Türkiye) Zn-Pb Yatağının Jeolojik, Mineralojik, Jeokimyasal ve Kökensel İncelemesi. Karadeniz Teknik Üniversitesi, Trabzon, 2003.

[6] Demir Y. Istala ve Köstere (Zigana/Gümüşhane) Cu-Pb-Zn Madenleri ve Yan Kayaçlarının Mineralojisi ve Dokusal Özelliklerinin Karşılaştırılmalı İncelenmesi. Yüksek Lisans Tezi, K.T.Ü. Fen Bilimleri Enstitüsü, Trabzon-Türkiye, 2005.

[7] Vural A, Aydal D. Soil geochemistry study of the listvenite area of Ayvacik (Çanakkale, Turkey). Casp J Environ Sci 2020; 18:205–215.

[8] Vural A. Evaluation of soil geochemistry data of Canca Area (Gümüşhane, Turkey) by means of Inverse Distance Weighting (IDW) and Kriging methods-preliminary findings. Bull Miner Res Explor 2018; 158:10–20.

[9] Vural A, Aydal D. Using soil geochemistry for gold exploration:Ayvacık (Çanakkale-Northwest Turkey). 34th National and the 2nd International Geosciences Congress. Tehran, Iran: 2016.

[10] Vural A. Investigation of the relationship between rare earth elements, trace elements, and major oxides in soil geochemistry. Environ Monit

Assess 2020; 192:124.
[11] Vural A, Erdoğan M. Eski Gümüşhane Kırkpavli Alterasyon Sahasında Toprak Jeokimyası. Gümüşhane Üniversitesi Fen Bilim Enstitüsü Derg 2014; 4:1–15.
[12] Reis AP, Sousa AJ, Cardoso Fonseca E. Soil geochemical prospecting for gold at Marrancos (Northern Portugual). J Geochemical Explor 2001; 73:1–10.
[13] Ketin İ, Canitez N. Yapısal Jeoloji. İstanbul İTÜ Kütüphanesi: 1972.
[14] Özsayar T, Pelin S, Gedikoğlu A. Doğu Pontidlerde Kretase. KTÜ Yer Bilim Derg 1981; 1:65–114.
[15] Bektaş O. Upper Cretaceous shoshonitic volcanism and its importance in the eastern Pontides. Karadeniz Tech Univ Earth Sci Bull 1984; 3:53–62.
[16] Bektaş O, Güven İH. Alaskan Aphinitic Type Ultramafic and Mafic Complexes as the Root Zone of the Eastern Pontide Magmatic Arc (NE Turkey). Geology of the Black Sea Region. Ankara, Türkiye: 1995:189–196.
[17] Topuz G, Altherr R, Kalt A, Satir M, Werner O, Schwarz WH. Aluminous granulites from the Pulur complex, NE Turkey: A case of partial melting, efficient melt extraction and crystallisation. Lithos 2004; 72:183–207.
[18] Topuz G, Altherr R, Siebel W, Schwarz WH, Zack T, Hasözbek A, Barth M, Satir M, Şen C. Carboniferous high-potassium I-type granitoid magmatism in the Eastern Pontides: The Gümüşhane pluton (NE Turkey). Lithos 2010; 116:92–110.
[19] Kaygusuz A, Aydınçakır E, Yücel C, Atay HE. Petrographic and geochemical characteristics of carboniferous plutonic rocks around Erenkaya (Gümüşhane, NE Turkey). J Eng Res Appl Sci 2021; 10:1774–1778.
[20] Vural A, Kaygusuz A. Petrology of the paleozoic plutons in Eastern pontides: artabel pluton (Gümüşhane, NE Turkey). J Eng Res Appl Sci 2019; 8:1216–1228.
[21] Kaygusuz A. Geochronological age relationships of Carboniferous Plutons in the Eastern Pontides (NE Turkey). J Eng Res Appl Sci 2020; 9:1299–1307.
[22] Karslı O, Dokuz A, Kandemir R. Subduction-related Late Carboniferous to Early Permian Magmatism in the Eastern Pontides, the Camlik and Casurluk plutons: Insights from geochemistry, whole-rock Sr–Nd and in situ zircon Lu–Hf isotopes, and U–Pb geochronology. Lithos 2016; 266–267:98–114.
[23] Kaygusuz A, Arslan M, Siebel W, Sipahi F, Ilbeyli N. Geochronological evidence and tectonic significance of Carboniferous magmatism in the southwest Trabzon area, eastern Pontides, Turkey. Int Geol Rev 2012; 54:1776–1800.
[24] Kaygusuz A, Arslan M, Sipahi F, Temizel İ. U–Pb zircon chronology and petrogenesis of Carboniferous plutons in the northern part of the Eastern Pontides, NE Turkey: Constraints for Paleozoic magmatism and geodynamic evolution. Gondwana Res 2016; 39:327–346.
[25] Çoğulu E. Gümüşhane ve Rize granitik plutonlarının mukayeseli petrojeolojik ve jeokronolojik etüdü. Unpubl Diss Thesis, İstanbul Tech Univ 1975.
[26] Yılmaz Y. Petrology and structure of the Gümüşhane Granite and surrounding rocks, North-Eastern Anatolia. PhD Thesis, Univ London 1972:260 p.
[27] Saydam Eker Ç. Petrography and geochemistry of Eocene sandstones from eastern Pontides (NE TURKEY): Implications for source area weathering, provenance and tectonic setting. Geochemistry Int 2012; 50:683–701.
[28] Ağar Ü. Geology of Demirözü (Bayburt) and Köse (Kelkit). KTU, Trabzon, 1977.
[29] Dokuz A, Karslı O, Chen B, Uysal I. Sources and petrogenesis of Jurassic granitoids in the Yusufeli area, Northeastern Turkey: Implications for pre- and post-collisional lithospheric thinning of the eastern Pontides. Tectonophysics 2010; 480:259–279.
[30] Ustaömer T, Robertson AHF, Ustaömer PA, Gerdes A, Peytcheva I. Constraints on variscan and cimmerian magmatism and metamorphism in the pontides (Yusufeli-Artvin area), NE Turkey from U-Pb dating and granite geochemistry. Geol Soc Spec Publ 2013; 372:49–74.
[31] Pelin S. Alucra (Giresun) Güneydoğu Yöresinin Petrol Olanakları Bakımından Jeolojik İncelenmesi. Karadeniz Tek Üniversitesi Yayınları 1977:87–103.
[32] Sipahi F, Vural A, Akpinar I, Saydam Eker Ç, Kaygusuz A. Comparison of Fluid Inclusions of Egrikar Fe-Cu, Kopuz Fe And Karadag Fe-Cu Skarns Occurrences (Gümüshane, Turkey). 3rd International Conference on Engineering and Natural Science I(CENS 2017). 2017:561–561.
[33] Temizel İ, Arslan M, Yücel C, Abdioğlu Yazar E, Kaygusuz A, Aslan Z. U-Pb geochronology, bulk-rock geochemistry and petrology of Late Cretaceous syenitic plutons in the Gölköy (Ordu) area (NE Turkey): Implications for magma generation in a continental arc extension triggered by slab roll-back. J Asian Earth Sci 2019; 171:305–320.

[34] Sipahi F, Saydam Eker Ç, Akpınar İ, Gücer MA, Vural A, Kaygusuz A, Aydurmuş T. Eocene magmatism and associated Fe-Cu mineralization in northeastern Turkey: a case study of the Karadağ skarn. Int Geol Rev 2022; 64:1530–1555.

[35] Vural A, Kaygusuz A. Petrographic and geochemical characteristics of late cretaceous volcanic rocks in the vicinity of Avliyana (Gümüşhane, NE Turkey). J Eng Res Appl Sci 2021; 10:1796–1810.

[36] Köprübaşı N, Şen C, Kaygusuz A. Doğu Pontid adayayı granitoyidlerinin karşılaştırılmalı petrografik ve kimyasal özellikleri, KD Türkiye. Uygulamalı Yerbilim Derg 2000; 1:111–120.

[37] Kaygusuz A, Saydam Eker Ç. Geochemical features and petrogenesis of Late Cretaceous subduction-related volcanic rocks in the Değirmentaşı (Torul/Gümüşhane) area, Eastern Pontides (NE Turkey). J Eng Res Appl Sci 2021; 10:1689–1702.

[38] Kaygusuz A, Arslan M, Temizel İ, Yücel C, Aydınçakır E. U–Pb zircon ages and petrogenesis of the Late Cretaceous I-type granitoids in arc setting, Eastern Pontides, NE Turkey. J African Earth Sci 2021; 174:104040.

[39] Kaygusuz A, Siebel W, Şen C, Satır M. Petrochemistry and petrology of I-type granitoids in an arc setting: The composite Torul pluton, Eastern Pontides, NE Turkey. Int J Earth Sci 2008; 97:739–764.

[40] Tokel S. Doğu Karadeniz Bölgesinde Eosen yaşlı kalk-alkalen andezitler ve jeotektonizma. Geol Soc Turkish Bulletion 1977; 20:49–54.

[41] Karslı O, Chen B, Aydın F, Şen C. Geochemical and Sr-Nd-Pb isotopic compositions of the Eocene Dölek and Sariçiçek Plutons, Eastern Turkey: Implications for magma interaction in the genesis of high-K calc-alkaline granitoids in a post-collision extensional setting. Lithos 2007; 98:67–96.

[42] Topuz G, Okay AI, Altherr R, Schwarz WH, Siebel W, Zack T, Satir M, Sen C. Post-collisional adakite-like magmatism in the Agvanis Massif and implications for the evolution of the Eocene magmatism in the Eastern Pontides (NE Turkey). Lithos 2011; 125:131–150.

[43] Kaygusuz A, Sipahi F, Ilbeyli N, Arslan M, Chen B, Aydınçakır E. Petrogenesis of the late Cretaceous Turnagöl intrusion in the eastern Pontides: Implications for magma genesis in the arc setting. Geosci Front 2013; 4:423–438.

[44] Aslan Z, Arslan M, Temizel İ, Kaygusuz A. K-Ar dating, whole-rock and Sr-Nd isotope geochemistry of calc-alkaline volcanic rocks around the Gümüşhane area: Implications for post-collisional volcanism in the Eastern Pontides, Northeast Turkey. Mineral Petrol 2014; 108:245–267.

[45] Kaygusuz A, Yücel C, Arslan M, Sipahi F, Temizel İ, Çakmak G, Güloglu ZS. Petrography, mineral chemistry and crystallization conditions of cenozoic plutonic rocks located to the north of Bayburt (Eastern Pontides, Turkey). Bull Miner Res Explor 2018; 157:75–102.

[46] Kaygusuz A, Merdan Tutar Z, Yücel C. Mineral chemistry, crystallization conditions and petrography of Cenozoic volcanic rocks in the Bahçecik (Torul/Gumushane) area, Eastern Pontides (NE Turkey). J Eng Res Appl Sci 2017; 6:641–651.

[47] Kaygusuz A, Gucer MA, Yücel C, Aydınçakır E, Sipahi F. Petrography and crystallization conditions of Middle Eocene volcanic rocks in the Aydıntepe-Yazyurdu (Bayburt) area, Eastern Pontides (NE Turkey). J Eng Res Appl Sci 2019; 8:1205–1215.

[48] Temizel İ, Arslan M, Yücel C, Abdioğlu Yazar E, Kaygusuz A, Aslan Z. Eocene tonalite–granodiorite from the Havza (Samsun) area, northern Turkey: adakite-like melts of lithospheric mantle and crust generated in a post-collisional setting. Int Geol Rev 2020; 62:1131–1158.

[49] Yücel C, Arslan M, Temizel İ, Abdioğlu Yazar E, Ruffet G. Evolution of K-rich magmas derived from a net veined lithospheric mantle in an ongoing extensional setting: Geochronology and geochemistry of Eocene and Miocene volcanic rocks from Eastern Pontides (Turkey). Gondwana Res 2017; 45:65–86.

[50] Sipahi F, Kaygusuz A, Saydam Eker Ç, Vural A, Akpınar İ. Late Cretaceous arc igneous activity: the Eğrikar Monzogranite example. Int Geol Rev 2018; 60:382–400.

[51] Vural A, Kaygusuz A. Geochronology, petrogenesis and tectonic importance of Eocene I-type magmatism in the Eastern Pontides, NE Turkey. Arab J Geosci 2021; 14.

[52] Aydınçakır E, Yücel C, Ruffet G, Gücer MA, Akaryalı E, Kaygusuz A. Petrogenesis of post-collisional Middle Eocene volcanism in the Eastern Pontides (NE, Turkey): Insights from geochemistry, whole-rock Sr-Nd-Pb isotopes, zircon U-Pb and 40Ar-39Ar geochronology. Geochemistry 2022:125871.

[53] Kaygusuz A, Şahin K. Mescitli (Torul / Gümüşhane) ve Çevresindeki Eosen Yaşlı Volkanik Kayaçların Petrografik, Jeokimyasal ve Petrolojik Özellikleri. Gümüşhane Üniversitesi

Fen Bilim Enstitüsü Derg 2016; 6:89.
[54] Kaygusuz A, Aslan Z, Aydınçakır E, Yücel C, Gücer MA, Şen C. Geochemical and Sr-Nd-Pb isotope characteristics of the Miocene to Pliocene volcanic rocks from the Kandilli (Erzurum) area, Eastern Anatolia (Turkey): Implications for magma evolution in extension-related origin. Lithos 2018; 296–299:332–351.
[55] Temizel İ, Abdioğlu Yazar E, Arslan M, Kaygusuz A, Aslan Z. Mineral chemistry, whole-rock geochemistry and petrology of Eocene I-type shoshonitic plutons in the Gölköy area (Ordu, NE Turkey). Bull Miner Res Explor 2018; 157:121–152.
[56] Güven İH. Doğu Pontidlerin 1/100.000 Ölçekli Kompilasyonu. Ankara: MTA Genel Müdürlüğü; 1993.
[57] Vural A, Kaygusuz A. Avliyana (Torul-Gümüşhane) Antimonit Cevherleşmesinin Jeolojisi-Mineralojisi ve Kökeninin Araştırılması. TÜBİTAK Ar-Ge 3001 Programı, Proje Sonuç Raporu (Proje No: 113Y382), Gümüşhane, Türkiye. 2016.
[58] Vural A, Kaygusuz A, Dönmez H. Avliyana Antimonit Cevherleşmesinin Duraylı İzotop ve Sıvı Kapanım Verileriyle Değerlendirilmesi. 69. Türkiye Jeoloji Kurultayı. Ankara, Türkiye: 2016:370–373.
[59] Vural A, Kaygusuz A. Paleozoyik Yaşlı Artabel Plütonunun (Gümüşhane) Petrografik ve Jeokimyasal Özellikleri. 3. Uluslararası GAP Matematik-Mühendislik-Fen ve Sağılık Bilimleri Kongresi. Şanlıurfa, Türkiye: İKSAD; 2019.
[60] Vural A. Zenginleştirilmiş Jeoturizm Rotası: Karadağ ve Artabel Gölleri. 71. Türkiye Jeoloji Kurultayı. Ankara, Türkiye: 2018:481–482.
[61] Güner S, Yazıcı EN, Dursun A, Yılmaz Z, Yılmaz H, Ağan A, Özgüner KC. Gümüşhane-Bayburt-Trabzon Polimetal Ruhsat Sahaları Jeoloji Raporu. Ankara, Türkiye: 2003.
[62] Vural A, Kaygusuz A. Kirlilik Parametrelerine Göre Farklı Kayaçların Element İçeriklerinin Araştırılması: Avliyana (Torul-Gümüşhane/Türkiye). 2. Uluslararası Hasankeyf Bilimsel Araştırmalar ve İnovasyon Kongresi, Batman, Türkiye: 2022:251–259.
[63] Vural A. K-Ar dating for determining the age of mineralization as alteration product: A case study of antimony mineralization vein type in granitic rocks of Gümüşhane area, Turkey. Acta Phys Pol A 2017; 132:792–795.
[64] Vural A. Zenginleştirilmiş Jeoturizm Güzergahlarına Dair Farkındalık Oluşturulması : Eski Gümüşhane - Dörtkonak Güzergahı [Creation of Awareness of Enhanced Geotourism Routes: Old Gümüşhane-Dörtkonak Route]. Gümüşhane Üniversitesi Sos Bilim Enstitüsü Elektron Derg 2019; 10:250–274.
[65] Vural A, Külekçi G. Zenginleştirilmiş Jeoturizm Güzergahı:Gümüşhane-Bahçecik Köyü (Enriched Geotourism Route: Gümüşhane-Bahçecik Village). Euroasia J Math Eng Nat Med Sci 2021; 8:1–23.
[66] Vural A, Kaygusuz A, Dönmez H, Yücel C. Geochemistry and Geochronology of the Avliyana Granitoid (Gümüşhane/Ne Turkey). 71. Türkiye Jeoloji Kurultayı. Ankara, Türkiye: Türkiye Jeoloji Kurultayı; 2018:391–392.
[67] Vural A, Çiçek B. Gümüştuğ Antimonit Cevherleşmesinin Toprak Jeokimyası ve Titrek Kavak (Populus Tremula)'nın Biyojeokimyasal Özelliklerinden Yararlanılarak Araştırılması. GÜBAP, Ar-Ge 1002, Proje Sonuç Raporu. Proje No:19.F5114.01.02, Gümüşhane, Türkiye: 2021.
[68] Mandelbrot BB. The Fractal Geometry of Nature (Updated and Augmented Edition). San Francisco, CA.: W.H. Freeman; 1983.
[69] Hassanpour S, Afzal P. Application of concentration–number (C–N) multifractal modeling for geochemical anomaly separation in Haftcheshmeh porphyry system, NW Iran. Arab J Geosci 2013; 6:957–970.
[70] Tobler WR. A computer model simulation of urban growth in the detroit region. Econ Geogr 1970; 46:234–240.
[71] Çiçek B. Gümüştuğ (Torul-Gümüşhane) Antimonit Cevherleşmesinin Toprak Jeokimyası Açısından İncelenmesi. Gümüşhane Üniversitesi, Fen Bilimleri Enstitüsü, 2019.
[72] Afzal P, Mirzaei M, Yousefi M, Adib A, Khalajmasoumi M, Zarifi AZ, Foster P, Yasrebi AB. Delineation of geochemical anomalies based on stream sediment data utilizing fractal modeling and staged factor analysis. J African Earth Sci 2016; 119:139–149.